

EUROPEAN ORGANIZATION FOR NUCLEAR RESEARCH

Addendum to the ISOLDE and Neutron Time-of-Flight Committee

IS532: Mass spectrometry of neutron-rich chromium isotopes into the $N = 40$ “island of inversion”

January 11, 2016

D. Atanasov¹, K. Blaum¹, S. George¹, F. Herfurth², M. Kowalska³, S. Kreim¹,
D. Lunney⁴, V. Manea³, Z. Meisel⁵, M. Mougeot⁴, D. Neidherr², M. Rosenbusch⁶,
L. Schweikhard⁶, A. Welker⁷, F. Wienholtz^{3,6}, R. N. Wolf¹, K. Zuber⁷

¹*Max Planck Institute for Nuclear Physics, Heidelberg, Germany*

²*GSI Helmholtzzentrum für Schwerionenforschung GmbH, Darmstadt, Germany*

³*CERN, Geneva, Switzerland*

⁴*CSNSM-IN2P3-CNRS, Université Paris-Sud, Orsay, France*

⁵*Department of Physics, University of Notre Dame, Indiana, USA*

⁶*Ernst-Moritz-Arndt-University, Greifswald, Germany*

⁷*Technical University, Dresden, Germany*

Spokespersons:

Susanne Kreim, skreim@cern.ch

Vladimir Manea, vladimir.manea@cern.ch

Contact person: Vladimir Manea, vladimir.manea@cern.ch

Abstract:

We propose to measure the masses of neutron-rich chromium isotopes up to ^{63}Cr in order to test the predictions of state-of-the-art shell-model and beyond-mean-field calculations in the so-called “ $N = 40$ island of inversion”. The previously measured nuclear binding energies in the chromium isotopic chain are not precise enough to constrain the available theoretical approaches, as shown by comparison to recent NSCL mass measurements. This addendum would benefit from the new availability of intense neutron-rich chromium beams at ISOLDE, as well as from already existing ISOLTRAP measurements of chromium isotopes up to $A = 59$. The higher-precision mass data would also provide crucial references for future mass measurements using in-flight techniques, which are less precise but can however access significantly more exotic nuclides.

Requested shifts: 13 shifts of chromium beams in one run with RILIS



1 Motivation

The evolution of nuclear structure between ^{48}Ca and ^{78}Ni (proton number $20 < Z < 28$ and neutron number $28 < N < 50$) has received increasing attention during the last years both from theory and experiment. Efforts have been concentrated around nuclides with neutron number corresponding to one of the closed neutron (sub-)shells obtained in the independent-particle model [1, 2].

One recent, well-known example is the case of ^{52}Ca , to which a series of gamma-spectroscopy [3] and more recently mass-spectrometry [4] and laser-spectroscopy [5, 6] experiments were dedicated. A relatively high energy of the first excited 2^+ state $E(2_1^+)$ [3] together with the enhanced empirical shell-gap value determined by ISOLTRAP [4] were presented as evidence for a new magic number $N = 32$. However, the theoretical description of the magnetic moments of $^{49,51}\text{Ca}$ required neutron excitations across the $N = 32$ gap [5]. The charge radii of calcium isotopes between $N = 28$ and $N = 32$ are also shown to increase significantly [6]. Both observations are at odds with the idea of a closed neutron shell in ^{52}Ca . In the case of ^{52}Ca , the full set of nuclear observables are thus required to build a consistent microscopic picture.

In the nickel isotopic chain ($Z = 28$) the case of ^{68}Ni has received wide attention. Experiments revealed properties typical of a doubly-magic nucleus (high $E(2_1^+)$ and low quadrupole transition probability $B(E2; 2_1^+ \rightarrow 0_1^+)$ [7]), coexisting with a 0_2^+ intruder configuration described as having a deformed structure [8]. The spectroscopy of $N = 40$ isotones towards the proton mid-shell also revealed that the spherical stability observed in the ground state of ^{68}Ni is quickly eroded when protons are removed from the $Z = 28$ core. Measurements of low $E(2_1^+)$ [9–11] and more recently high $B(E2; 2_1^+ \rightarrow 0_1^+)$ [12–15] values of iron and chromium isotopes reveal a region of nuclear collectivity emerging in the two chains around $N = 40$. The maximum collectivity was found in the chromium isotopic chain, with quadrupole deformation estimated from $B(E2\uparrow)$ at $\beta_2 \approx 0.3$ [16].

Moreover, an analogy was drawn [17] between the structural evolution of $N = 40$ isotones in the chromium region and the so-called “island of inversion”, which originally referred only to the onset of deformation of $N \approx 20$ isotones when removing protons from the $Z = 20$ core. This latter phenomenon was explained in the shell-model framework as the result of the reduction of the energy gap between the $\nu d_{3/2}$ and $\nu f_{7/2}$ effective single-particle levels (which creates the $N = 20$ shell), together with the proximity of the quadrupole partners $\nu f_{7/2}$ and $\nu p_{3/2}$, driving quadrupole correlations. A similar situation was suggested for the onset of deformation at $N \approx 40$: the reduction of the energy gap between the $\nu f_{5/2}$ and $\nu g_{9/2}$ levels (which creates the $N = 40$ sub-shell), together with the proximity of the quadrupole partners $\nu g_{9/2}$ and $\nu d_{5/2}$, quickly drives the collectivity of the $N \approx 40$ nuclides for $Z < 28$. Following this analogy, the region around ^{64}Cr has been called a second island of inversion [17].

The state-of-the-art theoretical approaches were confronted early on with the emerging set of $E(2_1^+)$ and $B(E2\uparrow)$ data in the iron and chromium isotopic chains. To achieve an accurate description of the experimental data by the nuclear shell model, a large-scale interaction (LNPS [17]) was developed, allowing neutron excitations not only within the pf shell but also to the $\nu g_{9/2}$ and $\nu d_{5/2}$ orbitals. Only once this extended valence space was established, a satisfactory description of the $E(2_1^+)$ and $B(E2\uparrow)$ data could

be obtained (see for example [15]). In the Hartree-Fock-Bogoliubov (HFB) framework, both the $N = 20$ and the $N = 40$ isotones in the corresponding “islands of inversion” are predicted to be spherical at the static mean-field level. As thoroughly discussed in a recent paper based on HFB calculations with the Gogny interaction [18], nuclear deformation is acquired in this case dynamically at the beyond-mean-field level. In what concerns the $N = 40$ isotones, the recent calculations give an excellent agreement with experiment for $Z > 28$, however for $Z < 28$ the theoretical $E(2_1^+)$ values are significantly higher than the experimental ones.

While the microscopic models for the chromium region are already constrained to some extent by the measured data in the region, two important questions remain: how the predictions of these models hold out for even more neutron-rich systems, approaching $N = 50$; how well these models describe other observables than the $E(2_1^+)$ and $B(E2\uparrow)$ values. Very recent RIKEN measurements of $E(2_1^+)$ values of ^{66}Cr and $^{70,72}\text{Fe}$ address the first of the two questions and the conclusion of the study is the need for an adjustment of the LNPS interaction in order to obtain an accurate shell-model description of the new data [19].

In what concerns the requirement for complementary observables, nuclear binding energies are a logical choice, because they are sensitive to the onset of deformation. The sudden increase of correlation energy along an isotopic chain usually introduces a change in the trend of the binding energy with neutron number. When computing a mass filter which is typically a finite-difference derivative of the binding-energy surface, one can observe significant shifts or kinks in the trend of the filter where a structural change occurs. Well-known, the onset of collectivity at $N = 60$ in the neutron-rich $A \approx 100$ nuclei is easily recognizable by an increase in the two-neutron separation energy [20].

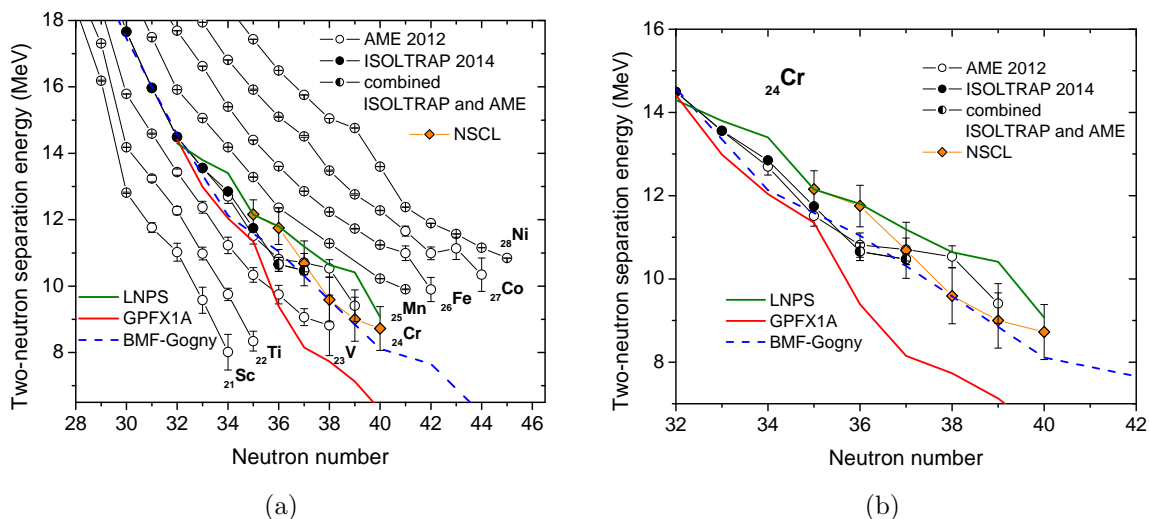


Figure 1: (a): Two-neutron separation energies in the region of interest, using data from AME2012 [20] (open circles), ISOLTRAP (full black circles), or combining AME and ISOLTRAP data (half-open circles). Orange diamonds mark data points determined using unpublished data from NSCL [21]. The lines represent the results of shell model calculations [22] with the LNPS (green line) the GPFX1A (red line) interaction, as well beyond-mean-field calculations using the Gogny interaction (dashed blue line) [23]. (b): Zoom on the chromium isotopic chain.

The two-neutron separation energies S_{2N} in the chromium region are shown in Fig. 1, using data from the atomic-mass evaluation [20], preliminary masses of chromium isotopes up to $N = 35$ measured in 2014 by ISOLTRAP and masses recently determined at NSCL [21]. Shown in Fig. 1 are also the results of shell-model calculations [22] using two interactions, LNPS and GXPF1A, as well as HFB calculations with the Gogny D1S interaction [23]. S_{2N} values determined from high-precision mass measurements are available until at least $N = 40$ in the isotopic chains between nickel and manganese. In the iron isotopic chain one does not observe any strong effect in the two-neutron separation energies, but rather a gradual curving of the trend upwards towards $N = 40$. A first sign of an onset of deformation was proposed for the manganese isotopic chain in [24] following ISOLTRAP mass measurements, however it is not clear whether the result is not due to an isomeric contamination of the ^{62}Mn data (hence the missing data point in Fig. 1). In the chromium isotopic chain the AME data across $N = 40$ are determined using the lower-precision TOFI facility at Los Alamos [25–27]. One notices that the S_{2N} trend determined by these values shows a flattening in the chromium isotopic chain between $N = 36$ and $N = 38$, which is typically an indication of an onset of deformation. However, the new NSCL data, although of higher uncertainty, draw a significantly different, much smoother trend. Comparing to theory, one notices the large deviation of the GXPF1A calculations from both the TOFI and NSCL data beyond $N = 36$, which is due to the missing $\nu g_{9/2}$ and $\nu d_{5/2}$ orbitals from the GXPF1A valence space. The LNPS calculation disagrees with the TOFI trend, as does the HFB calculation using the Gogny interaction. One notices that the effect of the preliminary ISOLTRAP masses is to smooth out the S_{2N} trend, an effect which might continue if further mass measurements are performed. The lack of high-precision mass references in the region also prevents further extension of the mass measurements by in-flight spectrometry methods, which although less precise can reach more exotic isotopes. This limitation is perfectly illustrated by the recent NSCL measurements, which have higher uncertainty than existing data. The precision of available experimental mass data is alone not sufficient to compare to the theoretical trends and higher-precision measurements are required. It would be important to test the LNPS predictions against the correct trend of ground-state binding energies, given that the interaction was tuned to reproduce primarily excited states. Higher precision data would also be required to test the predictions of the Gogny D1S calculations, which should be more reliable for the ground state, but have been so far mostly discussed with respect to the $E(2_1^+)$ states.

2 Experimental setup

The proposed measurements would be performed using the mass spectrometer ISOLTRAP [28], which now comprises a linear, radio-frequency quadrupole cooler and buncher (RFQ), a multi-reflection time-of-flight mass spectrometer (MR-TOF MS) and two Penning traps, one for preparation and one for precision mass spectrometry (see [29] for the most recent update on the ISOLTRAP setup). The MR-TOF MS is now routinely used at ISOLTRAP either as a beam purifier [30] or mass spectrometer [31], the latter application producing also the first mass measurements of calcium and potassium isotopes in the framework

of the IS532 experiment [4, 32]. ISOLTRAP possesses now two independent methods for mass determination. For yields as low as 10^2 ions per μC and half-lives larger than 100 ms, traditional Penning-trap mass spectrometry is the method of choice, while the MR-TOF MS acts as a fast beam purifier. For half-lives of a few hundred ms, multiple accumulations in the preparation Penning trap of MR-TOF-purified ion ensembles (stacking) can be applied, allowing to cope with higher contamination ratios [33]. In all these cases, the MR-TOF MS can be used with little additional experimental time to perform cross-check mass measurements, which are also a means of recording the beam composition. For ions of half-life in the 10-100 ms range and yield below 10 ions per μC , the MR-TOF MS becomes the superior mass-measurement tool. The relative precision achievable with the MR-TOF MS in the $A \approx 50$ region is close to 10^{-7} , sufficient for most nuclear-structure applications.

3 Beam-time request

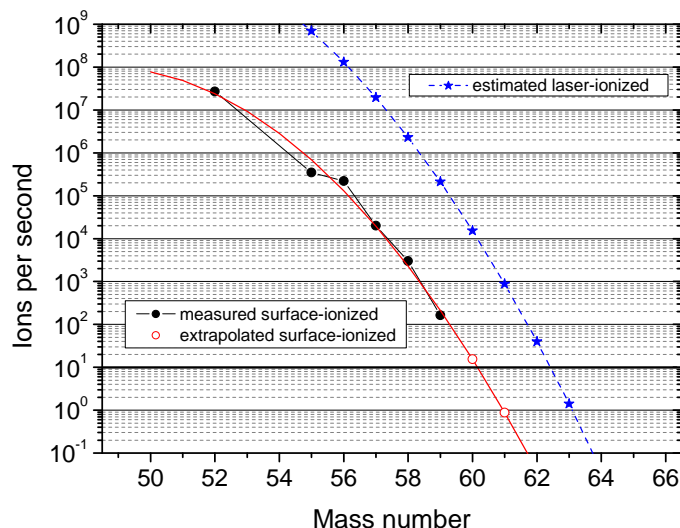


Figure 2: Yields of neutron-rich chromium isotopes estimated in 2014 by ISOLTRAP. The surface-ionized yields directly measured are marked by black circles, the yields with laser ionization, assuming a factor 10^3 enhancement, are given in blue stars.

We propose to measure the masses of $^{60-63}\text{Cr}$ with the mass spectrometer ISOLTRAP. We note that the $^{58-60}\text{Cr}$ were requested as part of the original IS532 proposal, but the request was put on hold, requiring beam development [34]. In the meantime a new ionization scheme for chromium has been developed and tested by the RILIS team [35]. In the 2014 experimental campaign, ISOLTRAP attempted to measure neutron-rich scandium isotopes as part of the IS532 program, using an uranium carbide target, without observing any scandium beam (stable or radioactive). In the absence of scandium, the allocated shifts were used to perform yield determinations and mass measurements of surface-ionized chromium isotopes up to ^{59}Cr , as well as to set-up RILIS on the new chromium ionization scheme. A test of the laser enhancement of the chromium yield was performed with ^{52}Cr ,

showing an enhancement by a factor greater than 800 [35]. A breakdown of the tantalum cavity of the target unit occurred before the laser enhancement could be tested using the MR-TOF MS. Still, the laser ionization efficiency was enough to allow measuring ^{59}Cr . The (order-of-magnitude) estimated yields obtained using the MR-TOF MS of ISOLTRAP are presented in Fig. 2, including an extrapolation to the isotopes of interest. An estimate of the expected yield with laser ionization, taking an enhancement of 10^3 , is also presented. Although the yield extrapolation does not consider the drop in chromium half-life and the unknown chromium release, a measurement of ^{63}Cr with the MR-TOF MS is feasible, which would already be sufficient to observe the evolution of two-neutron separation energies into the region of maximum collectivity.

Detailed shift request

The table below presents the detailed request of shifts of radioactive beam for the different isotopes. The number of requested shifts includes the time required for setting-up the measurement cycle of ISOLTRAP and for the identification in the precision Penning trap of reference isobars for MR-TOF mass measurements. The chromium yields are the estimated ones of Fig. 2.

Isotope	Half-life (ms) [36]	Yield (μC^{-1})	Target/ion source	Method	Shifts (8h)
^{60}Cr	490(10)	10^4	UC_x/RILIS	Penning trap	2
^{61}Cr	243(9)	10^3	UC_x/RILIS	Penning trap or MR-TOF MS	3
^{62}Cr	206(12)	$10^1 - 10^2$	UC_x/RILIS	MR-TOF MS	3
^{63}Cr	129(2)	$10^0 - 10^1$	UC_x/RILIS	MR-TOF MS	5
Total shifts of radioactive beam: 13					

Summary of requested shifts: 13 shifts of neutron-rich chromium beams from a UC_x target, with laser ionization;

References

- [1] O. Haxel, J. H. D. Jensen, H. E. Suess, *Phys. Rev.* **75**, 1766 (1949).
- [2] M. G. Mayer, *Phys. Rev.* **78**, 22 (1950).
- [3] A. Huck, *et al.*, *Phys. Rev. C* **31**, 2226 (1985).
- [4] F. Wienholtz, *et al.*, *Nature* **498**, 346 (2013).
- [5] R. F. Garcia Ruiz, *et al.*, *Phys. Rev. C* **91**, 041304 (2015).
- [6] R. F. Garcia Ruiz, *et al.*, *Nature Physics* in press.
- [7] O. Sorlin, *et al.*, *Phys. Rev. Lett.* **88**, 092501 (2002).
- [8] S. Suchyta, *et al.*, *Phys. Rev. C* **89**, 021301 (2014).
- [9] M. Hannawald, *et al.*, *Phys. Rev. Lett.* **82**, 1391 (1999).
- [10] O. Sorlin, *et al.*, *Eur. Phys. J. A* **16**, 55 (2003).
- [11] S. N. Liddick, *et al.*, *Phys. Rev. C* **87**, 014325 (2013).

- [12] J. Ljungvall, *et al.*, *Phys. Rev. C* **81**, 061301 (2010).
- [13] N. Aoi, *et al.*, *Phys. Rev. Lett.* **102**, 012502 (2009).
- [14] W. Rother, *et al.*, *Phys. Rev. Lett.* **106**, 022502 (2011).
- [15] H. L. Crawford, *et al.*, *Phys. Rev. Lett.* **110**, 242701 (2013).
- [16] B. Pritychenko, J. Choquette, M. Horoi, B. Karamy, B. Singh, *At. Data Nucl. Data Tables* **98**(4), 798 (2012).
- [17] S. M. Lenzi, F. Nowacki, A. Poves, K. Sieja, *Phys. Rev. C* **82**, 054301 (2010).
- [18] S. Pru, M. Martini, *The European Physical Journal A* **50**(5) (2014).
- [19] C. Santamaria, *et al.*, *Phys. Rev. Lett.* **115**, 192501 (2015).
- [20] M. Wang, *et al.*, *Chinese Phys. C* **36**, 1603 (2012).
- [21] Z. Meisel, private communication (2016), NSCL masses submitted for publication.
- [22] K. Sieja, private communication (2016), shell model calculations.
- [23] J. P. Delaroche, *et al.*, *Phys. Rev. C* **81**, 014303 (2010).
- [24] S. Naimi, *et al.*, *Phys. Rev. C* **86**, 014325 (2012).
- [25] X. Tu, *et al.*, *Z. Phys. A* **337**, 361 (1990).
- [26] H. Seifert, *et al.*, *Z. Phys. A* **349**, 25 (1994).
- [27] Y. Bai, D. J. Vieira, H. L. Seifert, J. M. Wouters, *AIP Conf. Proc.* **455**, 90 (1998).
- [28] M. Mukherjee, *et al.*, *Eur. Phys. J. A* **35**, 1 (2008).
- [29] S. Kreim, *et al.*, *Nucl. Instrum. Meth. B* **317**, 492 (2013).
- [30] R. Wolf, *et al.*, *Nucl. Instrum. Meth. A* **686**, 82 (2012).
- [31] R. Wolf, *et al.*, *Int. J. Mass Spectrom.* **349–350**, 123 (2013).
- [32] M. Rosenbusch, *et al.*, *Phys. Rev. Lett.* **114**, 202501 (2015).
- [33] M. Rosenbusch, *et al.*, *Appl. Phys. B* **114**, 147 (2014).
- [34] ‘Minutes of the 41st meeting of the isotope and neutron time-of-flight experiments committee’, CERN-INTC-2011-058, INTC-041 (2011).
- [35] T. Day Goodacre, *et al.*, *arXiv:1512.07875* (2015).
- [36] G. Audi, *et al.*, *Chinese Phys. C* **36**(12), 1157 (2012).

Appendix

DESCRIPTION OF THE PROPOSED EXPERIMENT

The experimental setup comprises: ISOLDE central beam line and ISOLTRAP setup. The ISOLTRAP setup has safety clearance, the memorandum document 1242456 ver.1 “Safety clearance for the operation of the ISOLTRAP experiment” by HSE Unit is released and can be found via the following link: <https://edms.cern.ch/document/1242456/1>.

Part of the	Availability	Design and manufacturing
ISOLTRAP setup	<input checked="" type="checkbox"/> Existing	<input checked="" type="checkbox"/> To be used without any modification